A Framework for Optimizing Multilevel AC Battery Energy Storage Systems

Alireza Ramyar
Electrical Engineering and Computer Science
University of Michigan
Ann Arbor, USA
aramyar@umich.edu

Jason B. Siegel
Mechanical Engineering
University of Michigan
Ann Arbor, USA
siegeljb@umich.edu

Al-Thaddeus Avestruz
Electrical Engineering and Computer Science
University of Michigan
Ann Arbor, USA
avestruz@umich.edu

2023 IEEE 24th Workshop on Control and Modeling for Power Electronics (COMPEL) | 979-8-3503-1618-6/23/$31.00 ©2023 IEEE | DOI: 10.1109/COMPEL52896.2023.10220997

***Abstract*—Battery energy storage systems (BESS) play an essential role in modern grids by supporting renewable power systems, improving grid power quality through voltage and frequency regulation, and supporting electric vehicle (EV) charging stations. At the same time, and with the rapid growth of EVs, an enormous number of EV batteries will be retired soon. These second-use EV batteries still have approximately 80% capacity and can be utilized in stationary applications like grid-connected BESSs to reduce the emissions from producing new batteries for energy storage systems. Directly producing multilevel AC from batteries reduces cost by eliminating the need for an explicit conventional inverter. In this paper, a framework is presented for optimizing the multilevel integration of power processing in BESSs, which is particularly applicable to BESSs with heterogeneous second-use batteries.**

***Index Terms*—battery energy storage systems, multilevel converters, partial power processing, second-use batteries, SOC balancing.**

I. Introduction

Battery energy storage systems (BESS) play important roles in grids, such as supporting renewable power systems, voltage and frequency regulation for grid power quality improvement, and supporting electric vehicle (EV) fast charging [1], [2]. Multilevel converters with integrated batteries are ideal architectures for grid-connected BESSs. Compared to conventional inverters with a high voltage dc bus, multilevel converters have better harmonic performance for the same switching frequency, which makes the required filters substantially smaller and cheaper [1], and are generally modular, which makes it possible to use smaller, lower voltage, and faster switches. Additionally, by integrating batteries in multilevel converters, energy storage capacitors can be eliminated from the structure, which also reduces costs. Furthermore, multilevel converters provide a higher degree of freedom for state-of-charge (SOC) balancing of the batteries, which is critical in BESSs [2]. Among Multilevel AC Battery Energy Storage Systems (MAC-BESS), architectures based on Cascaded H-Bridges (CHB) and Modular Multilevel Converters (MMC) are often used [1] with CHBs being among the best candidates [1], [2].

This work was supported in part by the Michigan Transportation Research and Commercialization (MTRAC) Grant CASE-283536 of the 21st Century Jobs Trust Fund received through the Michigan Strategic Fund (MSF) from the State of Michigan. The work was also supported in part by the National Science Foundation under CAREER Award No. 2146490.

At the same time, the rapid growth of retired EV batteries represents an excellent opportunity to utilize them in BESSs. There will be 200 GWh/y of used batteries from EVs [3] by 2030, which still have approximately 80% capacity [4] that could be used in grid-connected BESSs or other stationary applications. Thus, reusing these batteries in second-use battery energy storage systems (2-BESS) provides a sustainable solution that reduces the emissions from producing new batteries for energy storage systems and adds economic value to EV batteries. However, these second-use batteries have heterogeneous characteristics (such as capacity, voltage, and power capability), which causes some challenges that need to be addressed.

MMCs [5], [6] and CHBs [2], [7] with integrated batteries have been investigated in the literature. In [5], each sub-module includes one battery, one storage capacitor, one half-bridge, and one buck/boost indirect active interface (IAI), which connects the battery to the half-bridge. The sub-modules of [6] consists of one battery, one storage capacitor, one full-bridge, and one buck/boost IAI. These structures are suitable for applications where a common dc link exists and have more flexibility compared to CHB-based BESSs [1]. However, they need more active and passive components and have lower power efficiency than CHB-based BESSs [1]. In [7], each sub-module includes one battery and one full-bridge. In order to achieve SOC balancing, batteries are continuously sorted based on their SOCs, and then appropriate sub-modules are connected to the load. In [2], batteries rotate among different phases via a network of half-bridges and full-bridges in order to maintain SOC balancing for all three phases.

These MMC-based and CHB-based methods need online SOC estimation, have relatively complicated control schemes that cannot be easily generalized to other multilevel converters, and sometimes rely on redundant batteries and auxiliary circuits. Furthermore, they do not address the challenges of heterogeneous second-use batteries. This paper presents a framework for optimizing a general class of multilevel ac battery energy storage systems, which is particularly advantageous for systems with heterogeneous (e.g., second-use) batteries. In this

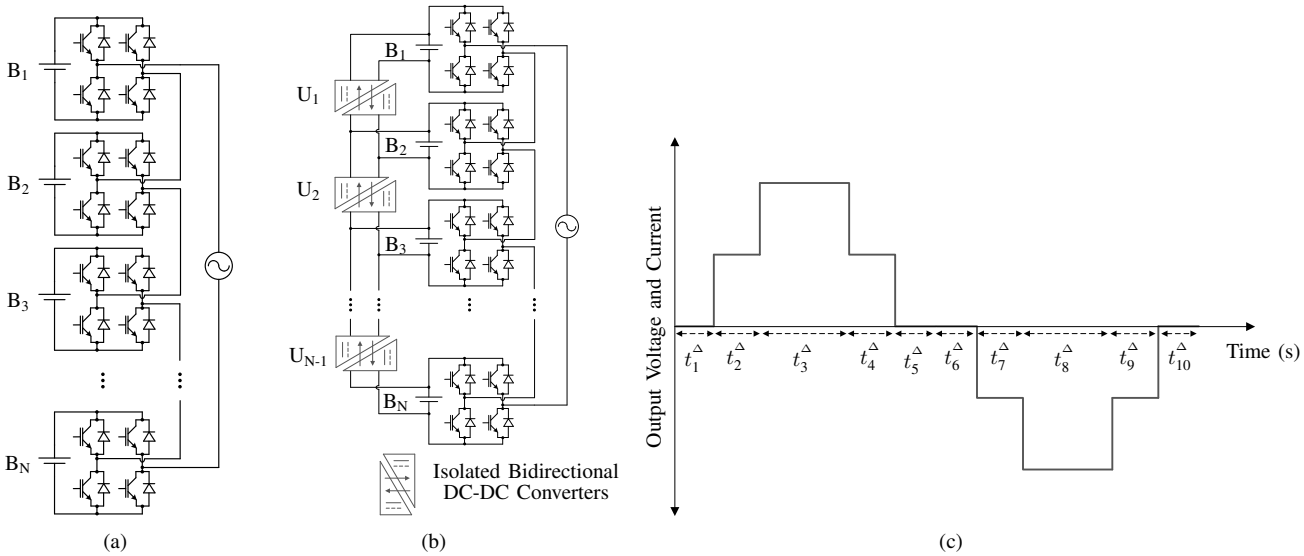

Fig. 1. (a) Conventional CHB inverter with integrated batteries. (b) CHB inverter with partial power processing converters. (c) Output voltage and current (for a resistive load) of a 5-level CHB inverter with SHE modulation.

paper, first, the framework is introduced; then, the optimization is formulated by employing the framework; and finally, the investigated framework is validated through Matlab simulation and then demonstrated via PLECS simulation.

II. Framework for Optimization

We investigate the optimization framework for the conventional CHB inverter, shown in Fig. 1(a), and the CHB inverter with adjuvant partial power processing converters (PPPC), shown in Fig. 1(b). In the latter case, isolated bidirectional dc-dc converters are added ($N-1$ converters, i.e., U_1 to $U_{N\text{-}1}$, for N batteries, i.e., B_1 to B_N) to process the mismatch power/energy among the batteries and enhance the utilization of the batteries. Additionally, we use selective harmonic elimination (SHE) [8] as the modulation technique. SHE is a simple fundamental frequency modulation scheme whose goal is to eliminate specific harmonics from the output voltage of the multilevel inverter and reduce its total harmonic distortion (THD). In principle, with N dc links and N H-bridges (HB), there are N degrees of freedom (switching angles) that can be utilized to eliminate $N-1$ harmonics and set the magnitude of the fundamental component. Figure 1(c) shows the output waveform (ac voltage and current) of a 5-level CHB inverter employing SHE modulation technique. In CHBs with SHE modulation and for N batteries, there exist N HBs, $2N+1$ voltage levels, and $4N+2$ time intervals (t_1^{Δ} to t_{4N+2}^{Δ}). For the case of Fig. 1(c), there are 2 batteries, 2 HBs, 5 voltage levels, 10 time intervals, and 1 PPPC (when used).

Although the framework is investigated for CHB inverters with SHE modulation, it can be generalized for other multilevel converters with various modulation techniques. Note that, in this paper, a resistive load is chosen to simplify the analysis. Now we are ready to introduce the notions of Charge-Vector and Charge-Matrix as two key components of the investigated framework.

A. Charge-Vector and Charge-Matrix

In the context of this investigation, a Battery Charge-Vector (*BCV*) is defined as an N-dimensional vector whose elements are the output charge of the batteries during the corresponding time intervals in the modulation. The Battery Charge-Matrix (*BCM*) is then defined as a matrix $Q^{\mathrm{B}}_{N\times(4N+2)}$ consisting of $4N+2$ *BCV*s to designate the output charge of the batteries during a complete ac cycle. For the case of Fig. 1(c) with the configuration of Fig. 1(a) or Fig. 1(b)

$$Q^{\mathrm{B}} = \begin{bmatrix} q^b_{1,1} & q^b_{1,2} & q^b_{1,3} & \cdots & q^b_{1,9} & q^b_{1,10} \\ q^b_{2,1} & q^b_{2,2} & q^b_{2,3} & \cdots & q^b_{2,9} & q^b_{2,10} \end{bmatrix}, \qquad (1)$$

where $q^b_{n,i}$ is the output charge of the n^{th} battery during the i^{th} time interval. Similarly, a Converter Charge-Vector (*CCV*) is defined as an $(N-1)$-dimensional vector, whose elements are the output charge of the converters during the corresponding time intervals, and the Converter-Charge-Matrix (*CCM*) is defined as a matrix $Q^{\mathrm{C}}_{(N-1)\times(4N+2)}$ consisting of $4N+2$ *CCV*s to designate the output charge of the converters during a complete ac cycle. For the case of Fig. 1(c) with the configuration of Fig. 1(b)

$$Q^{\mathrm{C}} = \begin{bmatrix} q^c_{1,1} & q^c_{1,2} & q^c_{1,3} & \cdots & q^c_{1,9} & q^c_{1,10} \end{bmatrix}, \qquad (2)$$

where $q^c_{m,i}$ is the output charge of the m^{th} converter during the i^{th} time interval.

As shown in Fig. 1(c), each time interval corresponds to a specific voltage level in the modulation. As an example, t_1^{Δ}, t_3^{Δ}, and t_7^{Δ} correspond to voltage levels of 0, 2, and -1, respectively. At each time interval and based on the corresponding voltage level, specific numbers of sub-modules are required to be connected to the load. For example, 0, 2, and 1 sub-modules must be connected to the load during t_1^{Δ}, t_3^{Δ}, and t_7^{Δ}, respectively. In the context of this investigation,

a Load Charge-Vector (*LCV*) is defined as an N-dimensional vector, which designates the connection of the sub-modules to the load during the corresponding time intervals. As an example, for $t_1^{\triangle}$ the only possible *LCV* is $[0\ 0]^{\mathrm{T}}$; at $t_3^{\triangle}$ the only possible *LCV* is $[q_3^l\ q_3^l]^{\mathrm{T}}$; and for $t_7^{\triangle}$, $[q_7^l\ 0]^{\mathrm{T}}$ and $[0\ q_7^l]^{\mathrm{T}}$ are two possible *LCV*s, where q_3^l and q_7^l are the charges transferred to the load by each sub-module connected to the load during time intervals $t_3^{\triangle}$ and $t_7^{\triangle}$, respectively. A Load Charge-Matrix (*LCM*) is then defined as a matrix $Q^{\mathrm{L}}_{N\times(4N+2)}$ consisting of $4N+2$ *LCV*s to designate the connection of the sub-modules to the load during a complete ac cycle, and the set of all the possible *LCM*s is called Load Charge-Matrix Space (*LCMS*). Note that all the *LCM*s in *LCMS* comply with the shape and phase of the output current. For instance, $\begin{bmatrix} 0 & q_2^l & q_3^l & q_4^l & 0 & 0 & 0 & q_8^l & q_9^l & 0 \\ 0 & 0 & q_3^l & 0 & 0 & 0 & q_7^l & q_8^l & 0 & 0 \end{bmatrix}$ and $\begin{bmatrix} 0 & 0 & q_3^l & q_4^l & 0 & 0 & q_7^l & q_8^l & 0 & 0 \\ 0 & q_2^l & q_3^l & 0 & 0 & 0 & 0 & q_8^l & q_9^l & 0 \end{bmatrix}$ are two possible *LCM*s for Fig. 1(c), where q_2^l, q_3^l, q_4^l, q_7^l, q_8^l, and q_9^l are the charges transferred to the load by each sub-module connected to the load during time intervals $t_2^{\triangle}$, $t_3^{\triangle}$, $t_4^{\triangle}$, $t_7^{\triangle}$, $t_8^{\triangle}$, and $t_9^{\triangle}$, respectively. It is worth noting that KCL enforces

$$Q^{\mathrm{L}} = Q^{\mathrm{B}}, \tag{3}$$

and

$$Q^{\mathrm{L}} = Q^{\mathrm{B}} + \begin{bmatrix} Q^{\mathrm{C}} \\ 0 \end{bmatrix} - \begin{bmatrix} 0 \\ Q^{\mathrm{C}} \end{bmatrix}, \tag{4}$$

in Fig. 1(a) and Fig. 1(b), respectively.

B. Optimization Design

In this investigation, a Gaussian statistical distribution is used for the capacity of the batteries. Additionally, we choose the current capability of the batteries to be limited to a certain C-rate (i.e., 0.1) relative to the battery's capacity at the time of the operation to manage the degradation of the batteries. For simplicity, the voltages of the batteries are assumed to be homogeneous (equal), which, together with the current capability of the batteries, leads to the statistical distribution of the power capability of the batteries. The goal of the optimization is to maximize the power utilization (U_{p}) and energy utilization (U_{e}) of the BESS. For a MAC-BESS, U_{p} is defined as the peak ac output power of the BESS normalized by the sum of the intrinsic power capability of the batteries. U_{e} is defined as the total extracted energy from the BESS prior to one of the batteries reaching its minimum allowed depth of discharge normalized by the sum of the available energy of the batteries. The decision variables are Q^{L}, Q^{B}, and Q^{C} (when used).

1) Without Partial Power Processing Converters: For a CHB inverter without PPPCs, shown in Fig. 1(a), U_{p} is the same for any given Q^{L}. In other words, the BESS output current is always limited by the current capability of the weakest battery, which is independent of Q^{L} (the connection of the sub-modules to the load). So, Monte Carlo simulations are performed to obtain the average U_{p} over the samples drawn from the power capability statistical distribution.

U_{e} can be optimized in a 2-step process as follows. Here, Q^{L} and Q^{B} are the decision variables. The goal is to minimize the deviation of individual SOCs from the average SOC, or in other words, make the battery SOCs closer to each other. All the batteries are assumed to have initial SOCs of 1 at the beginning of the first cycle, i.e., batteries are fully charged relative to their capacity at the time of the operation.

- *Optimization Formulation*

$$\min_{Q^{\mathrm{L}},Q^{\mathrm{B}}} \sum_{n=1}^{N} \left(\mathrm{SOC}_n - \overline{\mathrm{SOC}}\right)^2 \tag{5a}$$

$$\text{subject to :} \qquad \overline{\mathrm{SOC}} = \frac{\sum_{n=1}^{N} \mathrm{SOC}_n}{N}, \tag{5b}$$

$$\mathrm{SOC}_n = \frac{C_n - \langle \vec{\mathbf{1}}, Q^{\mathrm{B}}_{n,:} \rangle}{C_n}, \quad n = 1, 2, \cdots, N, \tag{5c}$$

$$Q^{\mathrm{L}} = Q^{\mathrm{B}}, \quad Q^{\mathrm{L}} \in \textit{LCMS}, \tag{5d}$$

where $\vec{\mathbf{1}}$ denotes the $(4N+2)$-dimensional all-ones vector, $\langle , \rangle$ denotes the inner product, N is the number of batteries, SOC_n is the SOC of the n^{th} battery at the end of one cycle (a scalar), $\overline{\mathrm{SOC}}$ is the average of $\mathrm{SOC}_1 \cdots \mathrm{SOC}_n$ (a scalar), C_n is the capacity of the n^{th} battery at the time of the operation (a scalar), and $Q^{\mathrm{B}}_{n,:}$ denotes the n^{th} row of Q^{B}. As mentioned in Section II-A, constraint (5d) enforces KCL. Additionally, $Q^{\mathrm{L}} \in \textit{LCMS}$ in constraint (5d) means that Q^{L} complies with the shape and phase of the output current. In the first step, we set the battery capacities to the expected values using the distribution flattening method [9] and find the Q^{L} that minimizes (5a). Note that, the objective function of (5a) is surrogate for $-1 \times U_{\mathrm{e}}$, meaning that optimizing one optimizes the other one too. To make the optimization tractable, we first select the best Q^{L} from a random subset of *LCMS*. We then perform a coordinate ascent around this Q^{L} until it converges to the local optimum Q^{L^*}.

In the second step, the elements of Q^{L} are fixed to the elements of Q^{L^*}, meaning that for each time interval, the same sub-modules as in Q^{L^*} are selected for Q^{L} to be connected to the load. We then perform Monte Carlo simulations to obtain the average U_{e} over the samples drawn from the capacity statistical distribution.

2) With Adjuvant Partial Power Processing Converters: For a CHB inverter with PPPCs, shown in Fig. 1(b), U_{e} of 100% is enforced by introducing suitable constraints into the optimization that ensures SOC balancing at the end of each ac cycle. Note that having the same SOCs for all the batteries at the end of each cycle is analogous to U_{e} of 100% because all the batteries reach their minimum allowed depth of discharge simultaneously. Again, all the batteries are assumed to have initial SOCs of 1 at the beginning of the first cycle. U_{p} is optimized in a 2-step process as follows. Here, the decision variables are Q^{L}, Q^{B}, and Q^{C}.

• *Optimization Formulation*

$$\max_{Q^{\mathrm{L}},Q^{\mathrm{B}},Q^{\mathrm{C}}} \sum_{n=1}^{N}\left(\sum_{i=1}^{4N+2} Q^{\mathrm{L}}_{n,i}\right) \tag{6a}$$

$$\text{subject to :} \quad -\left(\frac{P_n}{V}\right)T^{\triangle} \preceq Q^{\mathrm{B}}_{n,:} \preceq \left(\frac{P_n}{V}\right)T^{\triangle}, \tag{6b}$$

$$-\left(\frac{\mathcal{R}_{\mathrm{p}}}{V}\right)T^{\triangle} \preceq Q^{\mathrm{C}}_{m,:} \preceq \left(\frac{\mathcal{R}_{\mathrm{p}}}{V}\right)T^{\triangle}, \tag{6c}$$

$$\frac{\langle \vec{\mathbf{1}}, Q^{\mathrm{B}}_{n,:}\rangle}{C_n} = \frac{\langle \vec{\mathbf{1}}, Q^{\mathrm{B}}_{1,:}\rangle}{C_1}, \tag{6d}$$

$$Q^{\mathrm{L}} = Q^{\mathrm{B}} + \begin{bmatrix} Q^{\mathrm{C}} \\ 0 \end{bmatrix} - \begin{bmatrix} 0 \\ Q^{\mathrm{C}} \end{bmatrix}, \quad Q^{\mathrm{L}} \in \textit{LCMS}, \tag{6e}$$

$$\frac{Q^{\mathrm{C}}_{m,i}}{t^{\triangle}_i} = \frac{Q^{\mathrm{C}}_{m,1}}{t^{\triangle}_1}, \tag{6f}$$

$$\text{for all} 1 \le n \le N,\ 1 \le m \le N-1,\ 1 \le i \le 4N+2,$$

where $\vec{\mathbf{1}}$ denotes the $(4N+2)$-dimensional all-ones vector, V is the batteries' voltage (a scalar), $\mathcal{R}_{\mathrm{p}}$ is the upper bound for the power converter ratings (a scalar), and P_n is the power capability of the n^{th} battery (a scalar). $T^{\triangle}$ is a $(4N+2)$-dimensional vector containing all the time intervals defined as

$$T^{\triangle} = \begin{bmatrix} t^{\triangle}_1 & t^{\triangle}_2 & \cdots & t^{\triangle}_{4N+2} \end{bmatrix}. \tag{7}$$

Constraint (6b) limits the power capability of the batteries, and constraint (6c) limits the power converter ratings to an upper bound. Constraint (6d) enforces SOC balancing at the end of an ac cycle, and constraint (6e) enforces KCL. Again, $Q^{\mathrm{L}} \in \textit{LCMS}$ means that Q^{L} complies with the shape and phase of the output current.

In the first step, we set the battery capacities and power capabilities to the expected values using the distribution flattening method [9] and find the Q^{L} that maximizes (6a). Note that, the objective function of (6a) is surrogate for U_{p}. Again, to make the optimization problems tractable, we select the best Q^{L} from a random subset of *LCMS*. For each Q^{L}, a Linear Programming (LP) problem is solved; then, the optimal Q^{L} is selected among the solutions of LP problems to obtain the best objective function value (i.e., U_{p}). At the end of the first step, we perform a coordinate ascent around this Q^{L} until it converges to Q^{L^*}.

In the second step, the elements of Q^{L} are fixed to the elements of Q^{L^*}, meaning that for each time interval, the same sub-modules as in Q^{L^*} are selected for Q^{L} to be connected to the load. We then perform Monte Carlo simulations on the same optimization problem, i.e., (6), to obtain the average U_{p} over the samples drawn from the capacity and power capability statistical distributions. It is worth noting that each Monte Carlo instance is an LP problem.

Note that we select the upper bound for the power converter ratings, i.e., $\mathcal{R}_{\mathrm{p}}$, for each optimization instance. We sweep this bound relative to the sum of the intrinsic power capability of the batteries and repeat the entire process to find the tradeoff between the power converter rating (determined by converter processed power) and U_{p} (battery power capability that is utilized). Additionally, the PPPCs can be chosen to have either constant or variable power flow during an ac cycle; thus, we consider CHB with both variable PPPCs (VPPPC) and constant PPPCs (CPPPC) and compare the results. Constraint (6f) enforces the power converters to have constant power flow during an ac cycle. Note that this constraint is not enforced when we use VPPPCs.

3) Effect of Output Current's Magnitude and Phase: It is worth noting that we solve the optimization to obtain the maximum U_{p} of the BESS, which gives us the maximum output current that BESS can provide. To maintain the BESS maximum output current, the PPPCs should have certain output current values obtained from optimization. When the magnitude of the BESS output current changes, the output current of the PPPCs should follow the changes. Thus, in a BESS, the magnitude of the output current should be fed back to set the output currents of the PPPCs accordingly. The simulation results in the following Section demonstrate the effect of the output current's magnitude changes. Changing the output current's phase changes Q^{L} and consequently *LCMS*. However, the optimization formulations remain the same. We can solve the optimization for different phase values and make a lookup table. In a BESS, the output current's phase can be fed back to set the output current of the PPPCs to corresponding values from the lookup table.

III. Simulation Results

In order to evaluate the investigated framework, Monte Carlo simulations were performed in Matlab to compare the performance of CHB without PPPCs (with optimal Q^{L}), CHB with VPPPCs, and CHB with CPPPCs. Figures 1(a) and 1(b) show the schematics of the architectures for Monte Carlo simulations. Additionally, CHB with CPPPCs, shown in Fig. 1(b), was modeled and simulated in PLECS for full-load and half-load conditions. For all the Matlab and PLECS simulations, a 15-level (7 batteries) CHB inverter with SHE modulation and ac frequency of 60 Hz was used. For the batteries, we used the parameters of the battery modules in TESLA Model S EVs, i.e., 24 V and 250 Ah. Gaussian statistical distributions with μ_{capacity} of 1.00×250 Ah and σ_{capacity} of 0.10×250 Ah, 0.15×250 Ah, 0.20×250 Ah, and 0.25×250 Ah were used for the capacity of the batteries. The output voltage of the CHB is a 15-level ac waveform with a THD of 5.66 % and a fundamental component of 171 V peak (121 V rms). For simplicity, the load is assumed to be resistive, so the output voltage and current have the same shape and phase.

A. Optimization Results

In Fig. 2 and Fig. 3, normalized aggregate converter rating is defined as the sum of the ratings of the converters normalized by the sum of the intrinsic power capability of the batteries. Note that, for the economy of scale, all the converters are assumed to have the same rating, i.e., the highest rating among the converters.

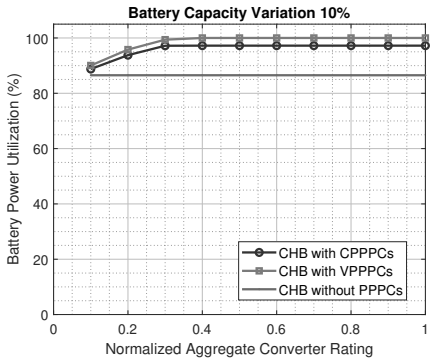

(a)

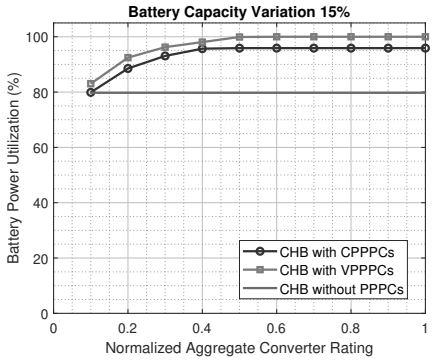

(b)

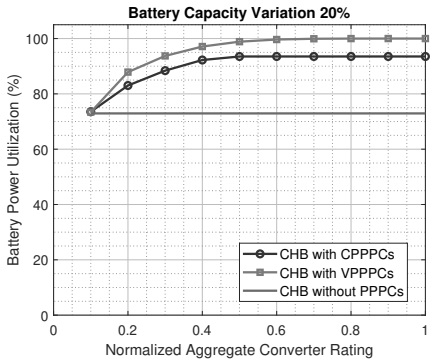

(c)

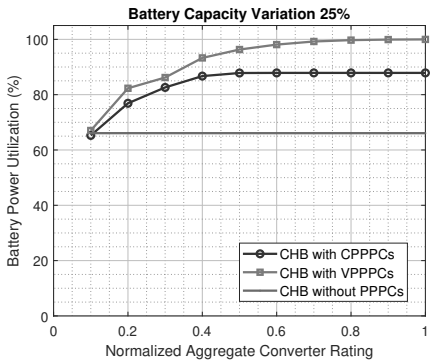

(d)

Fig. 2. Comparison of battery power utilization for CHB without PPPCs (with optimal Q^{L}), CHB with VPPPCs, and CHB with CPPPCs when heterogeneity is: (a) 10 % ($\mu_{\mathrm{capacity}} = 1\,\mathrm{p.u.}$, $\sigma_{\mathrm{capacity}} = 0.10\,\mathrm{p.u.}$), (b) 15 % ($\mu_{\mathrm{capacity}} = 1\,\mathrm{p.u.}$, $\sigma_{\mathrm{capacity}} = 0.15\,\mathrm{p.u.}$), (c) 20 % ($\mu_{\mathrm{capacity}} = 1\,\mathrm{p.u.}$, $\sigma_{\mathrm{capacity}} = 0.20\,\mathrm{p.u.}$), and (d) 25 % ($\mu_{\mathrm{capacity}} = 1\,\mathrm{p.u.}$, $\sigma_{\mathrm{capacity}} = 0.25\,\mathrm{p.u.}$).

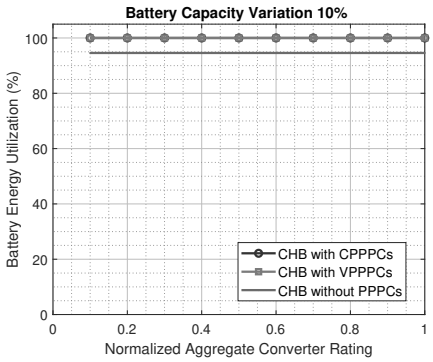

(a)

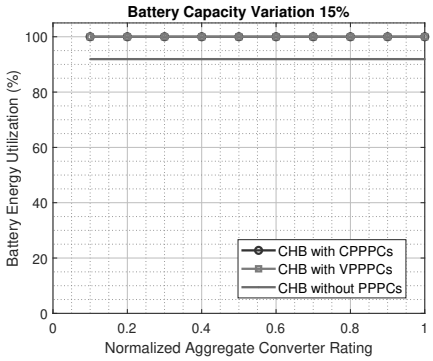

(b)

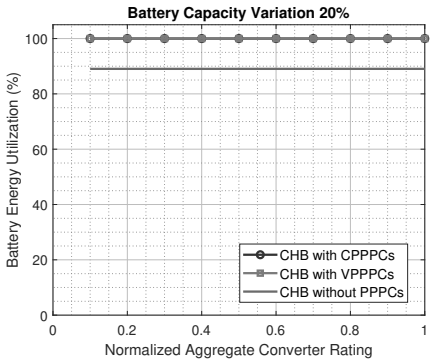

(c)

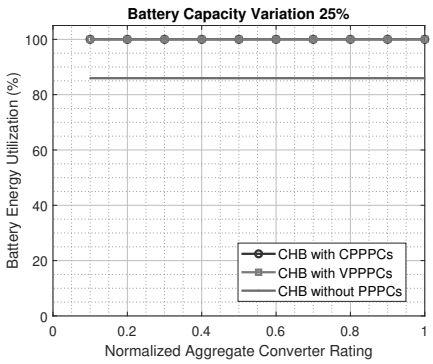

(d)

Fig. 3. Comparison of battery energy utilization for CHB without PPPCs (with optimal Q^{L}), CHB with VPPPCs, and CHB with CPPPCs when heterogeneity is: (a) 10 % ($\mu_{\mathrm{capacity}} = 1\,\mathrm{p.u.}$, $\sigma_{\mathrm{capacity}} = 0.10\,\mathrm{p.u.}$), (b) 15 % ($\mu_{\mathrm{capacity}} = 1\,\mathrm{p.u.}$, $\sigma_{\mathrm{capacity}} = 0.15\,\mathrm{p.u.}$), (c) 20 % ($\mu_{\mathrm{capacity}} = 1\,\mathrm{p.u.}$, $\sigma_{\mathrm{capacity}} = 0.20\,\mathrm{p.u.}$), and (d) 25 % ($\mu_{\mathrm{capacity}} = 1\,\mathrm{p.u.}$, $\sigma_{\mathrm{capacity}} = 0.25\,\mathrm{p.u.}$).

As shown, CHB with CPPPCs and VPPPCs show a better U_{p} than CHB without PPPCs. This superiority increases when the batteries become more heterogeneous, i.e., when the battery capacity variation increases, as illustrated in Fig. 4. Furthermore, CHB with CPPPCs and VPPPCs have U_{e} of 100 % for all the normalized aggregate converter ratings and all the battery capacity variation values, which is expected because SOC balancing is enforced by the constraints of the optimization. Although having the same SOC for all the batteries is desirable in BESSs, especially for stochastic loads, we can relax the SOC balancing constraints to increase U_{p}. This way, we can compromise between U_{e} and U_{p} based on the cost of batteries and power converters.

Additionally, CHB with VPPPCs has a better U_{p} than CHB with CPPPCs. This observation is also not surprising because the feasibility region of the optimization problem for CHB with CPPPCs is a subset of the feasibility region of the optimization problem for CHB with VPPPCs. Thus, for a given U_{p}, a higher power converter rating is needed for CPPPCs compared to the required converter rating of VPPPCs. As an example, for battery capacity variation of 20 % and at U_{p} of 92 %, the normalized aggregate converter rating for VPPPC and CPPPC is 0.28 and 0.4, corresponding to PPPCs with power ratings of 196 W and 280 W, respectively. However, faster converters are required for the VPPPCs. So, the choice of CPPPCs or VPPPCs is a tradeoff between processed power and the switching frequency of the converters and depends on the dynamics of the load. As a reference, for a CHB with SHE modulation and 7 batteries in a grid with ac frequency of 60 Hz, the switching frequency of the VPPPCs should be at least 30 KHz, which is straightforward for such small converters.

As shown in Fig. 4, when the battery capacity heterogeneity increases from 10 % (i.e., $\mu_{\text{capacity}} = 1\,\text{p.u.}$, $\sigma_{\text{capacity}} = 0.10\,\text{p.u.}$) to 25 % (i.e., $\mu_{\text{capacity}} = 1\,\text{p.u.}$, $\sigma_{\text{capacity}} = 0.25\,\text{p.u.}$), U_{p} decreases 7 %, 11 %, and 21 % for CHB with VPPPCs, CHB with CPPPCs, and CHB without PPPCs, respectively. Additionally, U_{e} decreases 9 % for CHB without PPPCs, while it always equals 100 % for CHB with VPPPCs and CHB with CPPPCs. This shows that CHB with VPPPCs and CPPPCs are also less impacted by increasing battery heterogeneity compared to CHB without PPPCs.

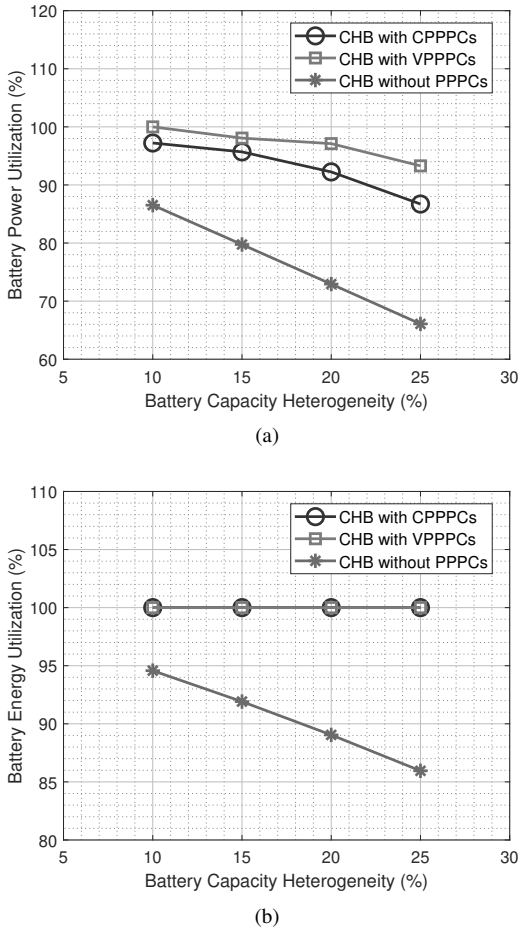

Fig. 4. Comparison of: (a) battery power utilization, and (b) battery energy utilization as a function of battery capacity heterogeneity for CHB without PPPCs (with optimal Q^{L}), CHB with VPPPCs, and CHB with CPPPCs. Normalized aggregate converter rating is 0.4 for CHB with VPPPCs and CHB with CPPPCs.

B. PLECS Simulation Results

A sample battery set was instantiated from the battery capacity statistical distribution for a battery supply with 20 % capacity variation. Then, by using the results of Section III-A, the power flow of the converters was optimized to obtain the maximum U_{p} for the case of CHB with CPPPCs at 0.4 normalized aggregate converter rating. The results were then used for the PLECS simulation to demonstrate the functionality of the structure. In the following simulations, the goal is to demonstrate that all the constraints (batteries' power limit, converters' power limit, batteries' SOC balancing constraints, and KCL constraints) are met in a circuit. C-Scripts were written in PLECS to generate the switching commands based on $Q^{\mathrm{L}*}$.

1) Full Load: Figures 5 and 6 show the results of the PLECS simulation for the full load case. As shown, the output voltage of the CHB is a 15-level ac waveform with a fundamental component of 171 V peak (121 V rms). For the instantiated battery set, the BESS current capability is 25.24 A, which is approximately 0.1×250 A. Note that the C-rates of the batteries were set to 0.1 relative to the batteries' capacity at the time of the operation. For a MAC-BESS, the BESS current capability is defined as the sum of the intrinsic power capability of the batteries over the peak of the multilevel output voltage, i.e., $24\,\text{V} \times 7$. From Fig. 5(b), U_{p} equals $\frac{23.41\,\text{A} \times 24\,\text{V} \times 7}{25.24\,\text{A} \times 24\,\text{V} \times 7} = 92.75\%$, which approximately equals U_{p} in Fig. 2(c), i.e., 92.24 %. Recall that 92.24 % is the average U_{p} over Monte Carlo simulations. As shown in Figures 5(c) and 6, the currents of the PPPCs and batteries are always below their limits. Furthermore, all the batteries have the same SOC trajectory, which shows that the batteries will be discharged simultaneously, and U_{e} is 100 %.

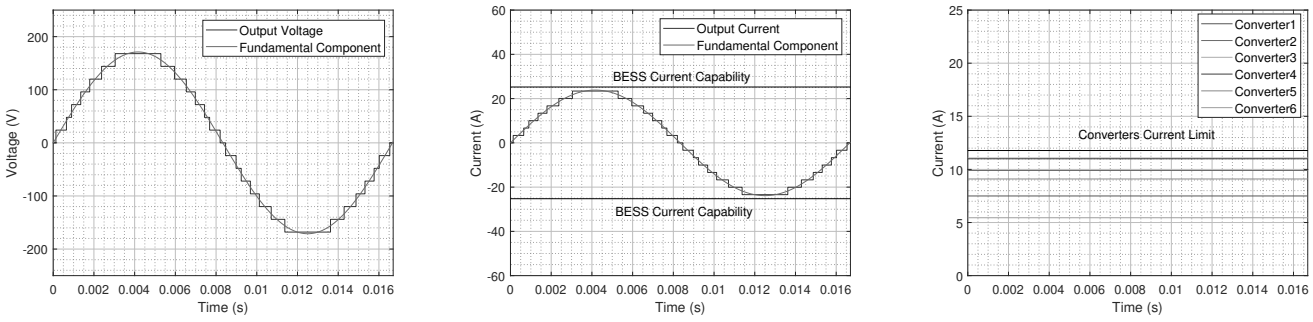

(a) (b) (c)

Fig. 5. PLECS simulation results for full load: (a) output voltage of the BESS, (b) output current of the BESS, and (c) output current of the converters.

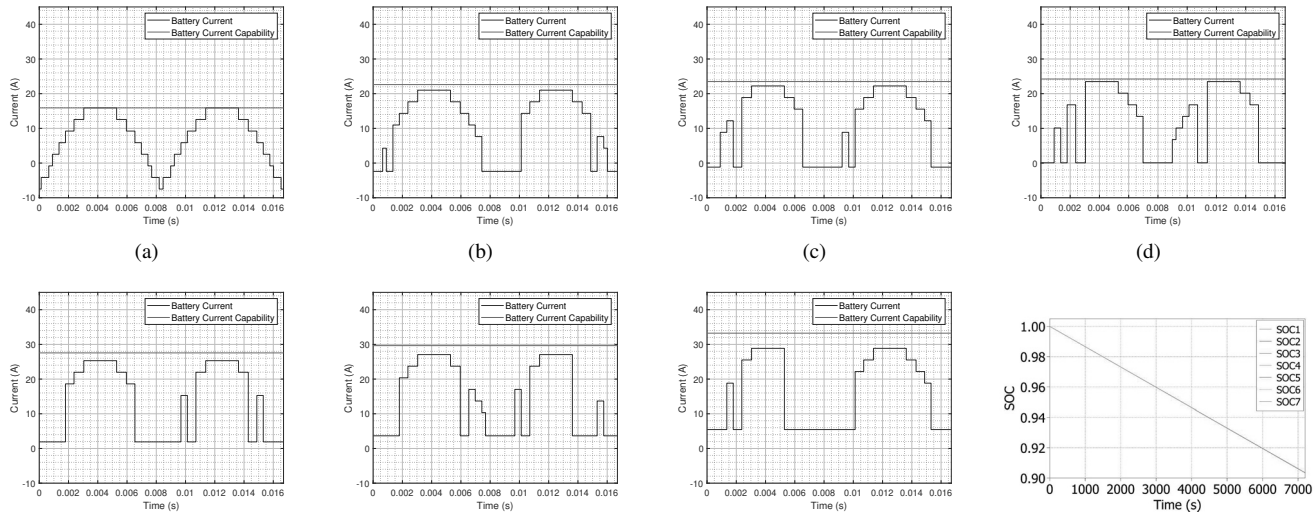

(a) (b) (c) (d)

(e) (f) (g) (h)

Fig. 6. PLECS simulation results for full load: current of (a) battery 1 (the weakest battery), (b) battery 2, (c) battery 3, (d) battery 4, (e) battery 5, (f) battery 6, (g) battery 7 (the strongest battery), and (h) SOC of batteries.

2) Half Load: Figures 7 and 8 show the result of the PLECS simulation for the half load case. In this simulation, the BESS output current's peak value is set to half of the BESS output current's peak value of the previous simulation, i.e., the full load case; consequently, the PPPCs' output currents were halved. As shown, the output voltage of the CHB is a 15-level ac waveform with a fundamental component of 171 V peak (121 V rms). Additionally, the currents of the PPPCs and batteries are always below their limits, as illustrated in Figures 7(c) and 8. Furthermore, all the batteries have the same SOC trajectory, which shows that the batteries will be discharged simultaneously, and U_{e} is 100 %. Although the batteries discharge slower than the full load case, U_{e} does not change when the magnitude of the output current changes. In this case, U_{p} equals $\frac{11.70\,\mathrm{A}\times 24\,\mathrm{V}\times 7}{25.24\,\mathrm{A}\times 24\,\mathrm{V}\times 7} = 46.35\%$, which is half of U_{p} for the full load case, i.e., 92.75 %. As mentioned in Section II-B3, U_{p} obtained from optimization gives us the maximum output current that BESS can provide, which we termed full load. When the output current decreases from this maximum value, U_{p} drops.

IV. Conclusion

This paper investigates a framework for optimizing multilevel ac battery energy storage systems. Through our simulation validation, we showed that by adding partial power processing converters to a multilevel inverter, optimizing the power flow of these converters, and optimizing the switching sequence of the inverter's sub-modules, we could achieve perfect SOC balancing among the batteries while maximizing the output power of the battery energy storage system. Furthermore, the functionality of the proposed structure and framework was demonstrated through simulation.

References

[1] G. Liang, H. D. Tafti, G. G. Farivar, J. Pou, C. D. Townsend, G. Konstantinou, and S. Ceballos, "Analytical derivation of intersubmodule active power disparity limits in modular multilevel converter-based battery energy storage systems," *IEEE Transactions on Power Electronics*, vol. 36, no. 3, pp. 2864–2874, 2020.

[2] A. Bani-Ahmad and C. A. Ooi, "Optimal cell utilization for improved power rating and reliability in a grid-scale three-phase battery energy storage system using hybrid modular multilevel converter topology with-

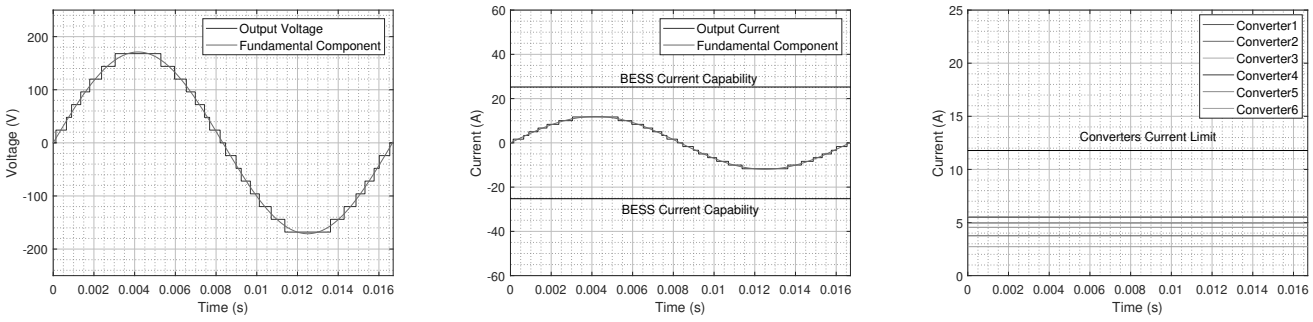

(a) (b) (c)

Fig. 7. PLECS simulation results for half load: (a) output voltage of the BESS, (b) output current of the BESS, and (c) output current of the converters.

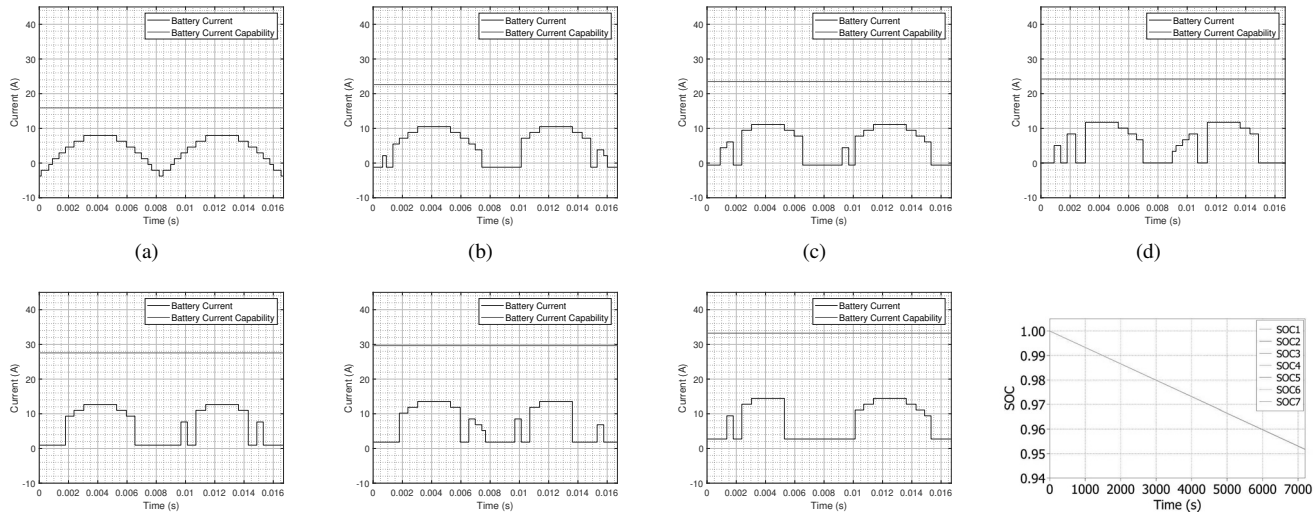

(a) (b) (c) (d)

(e) (f) (g) (h)

Fig. 8. PLECS simulation results for half load: current of (a) battery 1 (the weakest battery), (b) battery 2, (c) battery 3, (d) battery 4, (e) battery 5, (f) battery 6, (g) battery 7 (the strongest battery), and (h) SOC of batteries.

out redundant cells," *IEEE Journal of Emerging and Selected Topics in Power Electronics*, vol. 9, no. 2, pp. 1780–1794, 2019.

[3] H. Engel, P. Hertzke, and G. Siccardo, "Second-life EV batteries: The newest value pool in energy storage," McKinsey Center for Future Mobility, Global Editorial Services, Tech. Rep., 2019.

[4] E. Hossain, D. Murtaugh, J. Mody, H. M. R. Faruque, M. S. H. Sunny, and N. Mohammad, "A comprehensive review on second-life batteries: current state, manufacturing considerations, applications, impacts, barriers & potential solutions, business strategies, and policies," *IEEE Access*, vol. 7, pp. 73 215–73 252, 2019.

[5] M. Vasiladiotis and A. Rufer, "Analysis and control of modular multilevel converters with integrated battery energy storage," *IEEE Transactions on Power Electronics*, vol. 30, no. 1, pp. 163–175, 2014.

[6] Q. Chen, R. Li, and X. Cai, "Analysis and fault control of hybrid modular multilevel converter with integrated battery energy storage system," *IEEE Journal of Emerging and Selected Topics in Power Electronics*, vol. 5, no. 1, pp. 64–78, 2016.

[7] E. Chatzinikolaou and D. J. Rogers, "Cell SoC balancing using a cascaded full-bridge multilevel converter in battery energy storage systems," *IEEE Transactions on Industrial Electronics*, vol. 63, no. 9, pp. 5394–5402, 2016.

[8] M. S. Dahidah, G. Konstantinou, and V. G. Agelidis, "A review of multilevel selective harmonic elimination PWM: formulations, solving algorithms, implementation and applications," *IEEE Transactions on Power Electronics*, vol. 30, no. 8, pp. 4091–4106, 2014.

[9] X. Cui, A. Ramyar, P. Mohtat, V. Contreras, J. B. Siegel, A. G. Stefanopoulou, and A.-T. Avestruz, "Lite-sparse hierarchical partial power processing for second-use battery energy storage systems," *IEEE Access*, vol. 10, pp. 90 761–90 777, 2022.